

# Mutation in the Core Structure of Desmin Intermediate Filaments Affects Myoblast Elasticity

Catherine Even,<sup>1,\*</sup> Gilles Abramovici,<sup>1</sup> Florence Delort,<sup>2</sup> Anna F. Rigato,<sup>3</sup> Virginie Bailleux,<sup>1</sup> Abel de Sousa Moreira,<sup>1</sup> Patrick Vicart,<sup>2</sup> Felix Rico,<sup>3</sup> Sabrina Battonnet-Pichon,<sup>2</sup> and Fatma Briki<sup>1,\*</sup>

<sup>1</sup>Laboratoire de Physique des Solides, CNRS, Université Paris Sud, Université Paris-Saclay, Orsay, France; <sup>2</sup>Unité de Biologie Fonctionnelle et Adaptative, UMR 8251, CNRS, Université Paris Diderot, Sorbonne Paris Cité, Paris, France; and <sup>3</sup>Bio AFM Lab, U1006, Inserm, Aix-Marseille Université, Marseille, France

**ABSTRACT** Elastic properties of cells are mainly derived from the actin cytoskeleton. However, intermediate filaments are emerging as major contributors to the mechanical properties of cells. Using atomic force microscopy, we studied the elasticity of mouse myoblasts expressing a mutant form of the gene encoding for desmin intermediate filaments, p.D399Y. This variant produces desmin aggregates, the main pathological symptom of myofibrillar myopathies. Here we show that desmin-mutated cells display a 39% increased median elastic modulus compared to wild-type cells. Desmin-mutated cells required higher forces than wild-type cells to reach high indentation depths, where desmin intermediate filaments are typically located. In addition, heat-shock treatment increased the proportion of cells with aggregates and induced a secondary peak in the distribution of Young's moduli. By performing atomic force microscopy mechanical mapping combined with fluorescence microscopy, we show that higher Young's moduli were measured where desmin aggregates were located, indicating that desmin aggregates are rigid. Therefore, we provide evidence that p.D399Y stiffens mouse myoblasts. Based on these results, we suggest that p.D399Y-related myofibrillar myopathy is at least partly due to altered mechanical properties at the single-cell scale, which are propagated to the tissue scale.

## INTRODUCTION

Mechanical properties of cells play a key role in their behavior: for instance, in cell shape or cellular migration processes. From a physical point of view, a cell is a viscoelastic material. At timescales of seconds to tens of milliseconds, cells behave mostly as elastic solids (1). Cell elasticity is mainly determined by the cytoskeleton, which is a network formed by three types of polymeric filaments: actin, microtubules, and intermediate filaments (IFs) (2). Studies of cell mechanics have mainly focused on the role of actin filaments and microtubules. Actin plays a major role; in contrast, the role of microtubules is negligible (1,3). The implications of IFs remain to be determined, but they have recently become central in studies of the viscoelastic properties of cells (4–7).

Five main subtypes form the IF family (types I–V), all of which share a common tripartite organization characterized by a central  $\alpha$ -helical coiled-coil-forming region

(rod-domain) and two non- $\alpha$ -helical regions (“head” and “tail”) with variable lengths and sequences (8). Except for nuclear lamin (type-V IF), which is present in all tissues, IFs mainly exhibit tissue- or cell-specific expression; for example, fibroblasts express vimentin and epithelial cells express cytokeratin. However, different IFs display diverse characteristics such as mechanosensitivity, strength, and deformability (9).

Few studies have investigated the direct contribution of IFs to cell elasticity (7,10). Several methods can measure cell elasticity, including cell poker (11,12), pipette suction (13,14), scanning acoustic microscopy (15), and atomic force microscopy (AFM) techniques. AFM is widely used (10,16) and has numerous advantages, including high spatial resolution, excellent sensitivity, and fast time resolution. Many AFM methods that determine cell elasticity measure Young's modulus (7,16–18).

Initial studies of the elasticity of cancerous cells used AFM to show that cancerous cells are softer than noncancerous cells (19,20). However, further studies revealed that the correlation between cell mechanics and cancer is much more complex and that, in some cases, cancer cells are more rigid (21,22). Recently, AFM studies showed

Submitted November 16, 2016, and accepted for publication June 9, 2017.

\*Correspondence: [catherine.even@u-psud.fr](mailto:catherine.even@u-psud.fr) or [fatma.briki@u-psud.fr](mailto:fatma.briki@u-psud.fr)

Gilles Abramovici and Florence Delort contributed equally to this work.

Editor: Cecile Sykes.

<http://dx.doi.org/10.1016/j.bpj.2017.06.020>

© 2017 Biophysical Society.



that keratin IFs largely contribute to keratinocyte resilience (7). Keratinocytes lacking keratin are much softer than wild-type (WT) cells. Accordingly, keratin expression in keratin-deficient cells restores their mechanical properties similarly to those of WT cells.

Among type-III IFs, most studies focus on vimentin. Pioneering experiments on *in vitro* vimentin filaments highlight their ability to undergo severe deformation without breaking (9). Another type-III IF, desmin, is specifically expressed in muscle cells. Although desmin and vimentin share structural similarities, *in vitro* experiments show that they display distinct mechanical properties that are adapted to their respective cellular contexts (muscle or fibroblast) (23). Hence, the effect of desmin on the mechanical properties of cells remains less well documented.

To date, ~70 mutations in the desmin gene are attributed as causal in the most studied subgroup of myofibrillar myopathies, also called desminopathies. These diseases affect cardiac and skeletal muscles and are mainly characterized by the presence of desmin-rich aggregates in muscle (24). Most are missense mutations affecting the 2B region of the protein rod domain, leading to desmin network disorganization (25).

Patients with the p.D399Y mutation present severe lower limb muscle weakness and heart and respiratory failure. Additionally, *in vitro* experiments have characterized oligomer formation, filament assembly pathways, single filament nanomechanics, and network rheology for p.D399Y. For instance, viscosity measurements on gels of *in vitro* polymerized desmin filaments show that p.D399Y filaments are more viscous than WT desmin filaments (26), even in the case of WT-D399Y copolymerization. This suggests that p.D399Y has a dominant negative effect on the mechanics of WT desmin protein networks. Moreover, this mutation has a highly aggregative behavior in transient overexpression experiments (25) and in response to external stress, such as oxidative or heat-shock stress in C2C12 undifferentiated myoblasts (27). We previously showed that C2C12 myoblasts expressing p.D399Y that are cyclically stretched through an elastic substrate (4) present altered dynamics compared to cells expressing WT desmin. Indeed, at the end of a stretch, WT desmin cells reorient and elongate, whereas mutated desmin cells are much less affected. These results may be related to reduced flexibility of mutated desmin cells compared to WT desmin cells. In the current study, we explored the consequences of desmin pathogenic mutation p.D399Y on myoblast elasticity with AFM experiments.

We also investigated the contribution of desmin aggregates to such mechanical alteration, using heat-shock treatment to stimulate aggregate formation in cells expressing mutated desmin. Overall, this study indicates that cell elasticity change is dependent on the desmin network, which is affected by p.D399Y mutation (28).

## MATERIALS AND METHODS

### Cell culture

*In vitro* experiments used C2C12 myoblasts, which express endogenous desmin. To study the role of IFs in myoblast mechanics, we used a cell model of desminopathy based on C2C12 myoblasts stably expressing either exogenous human Myc-tagged WT desmin (DesWT) or desmin with the p.D399Y mutation (DesMUT). Detailed procedures for stable clone preparation were described previously (27). The Myc-tag allowed discrimination of human exogenous desmin (WT or mutant) from murine endogenous WT desmin, especially in immunofluorescence experiments. Moreover, as Myc is located at the N-terminal of the desmin protein, it does not interfere with polymerization (unlike the C-terminal, which increases aggregation). Importantly, the Myc-tag did not alter desmin network patterns for DesWT or DesMUT cells (Fig. S1).

C2C12 cells were cultivated in Dulbecco's Modified Eagle medium (D-MEM; Life Technologies, Carlsbad, CA) supplemented with 10% PAA Laboratories fetal bovine serum (GE Healthcare Biosciences, Pittsburgh, PA), 50 units/mL penicillin, and 50  $\mu$ g/mL streptomycin (Life Technologies). DesWT and DesMUT cells were cultivated in D-MEM (Life Technologies) supplemented with 20% PAA Laboratories fetal bovine serum (GE Healthcare Biosciences), 50 units/mL penicillin, and 50  $\mu$ g/mL streptomycin (Life Technologies). To maintain clone selection, 1 mg/mL Geneticin (Euromedex, Strasbourg, France) and 2  $\mu$ g/mL puromycin (Euromedex) were added to the medium. We added 5  $\mu$ g/mL doxycycline (Sigma-Aldrich, St. Louis, MO) to induce desmin expression. All cells were cultivated at 37°C in 5% CO<sub>2</sub>. Cells were subcultured every 72–96 h. For AFM experiments, we used a specific medium that did not require CO<sub>2</sub>, which provided pH stability (29).

When applicable, cells were heat-shocked 48 h after induction of desmin expression by incubation in a 42°C water bath for 2 h (27), followed by a 24 h recovery in fresh complete medium before AFM experiments.

### Immunofluorescent staining

For immunofluorescent staining, cells were cultivated on glass slides, fixed in 2% paraformaldehyde solution for 20 min at room temperature, and permeabilized with 0.5% Triton X-100 solution for 15 min. Afterwards, cells were incubated for 1 h with 1:100 anti-Myc mouse primary antibody (9E10; Santa Cruz Biotechnology, Dallas, TX) to stain Myc-tagged exogenous desmin or anti-desmin mouse primary antibody (D33; Dako, Agilent, Santa Clara, CA). Finally, cells were incubated for 45 min with 1:1000 Alexa Fluor 488 goat anti-mouse serum (A11029; Life Technologies) and 1:1000 Hoechst nuclear dye (Sigma-Aldrich). All antibodies were diluted in phosphate-buffered saline. Cells were mounted using Fluoromount G mounting medium (Interchim, Montluçon, France) and visualized with a LSM 700 confocal microscope (Carl Zeiss AG, Oberkochen, Germany) using Zen 2013 software (Carl Zeiss AG).

### Elasticity measurements with AFM

Elasticity of cells was measured using a Bioscope Digital Instruments D3100 AFM (Veeco Instruments, Plainview, NY) mounted on an inverted microscope.

Colloidal probes with 10  $\mu$ m-diameter borosilicate glass beads were purchased from Novascan (Ames, IA). We used colloidal probes, cantilevers featuring a sphere rather than a sharp tip for several reasons. First, the probes apply lower local pressure due to the larger contact surface, causing less cell damage. Moreover, contact area with the sample is higher, providing two advantages: it better follows the Hertz model (see below), and it obtains a partial average on the cell. Before each experiment, the spring constant of each cantilever was calibrated using the thermal noise method (30). Obtained values were of the order of 0.1 N/m.

Cells were adherent to the bottom of treated polystyrene tissue culture dishes. Before each experiment, cell medium was replaced with prewarmed CO<sub>2</sub>-independent medium (29), which avoided pH variations, allowing the sample to be in contact with air for ~2 h. All experiments were conducted at room temperature as it is sometimes done in the literature (7). The medium prewarmed to 37°C was kept at room temperature for ~2 h during indentation experiments. Indenting at room temperature does not seem to affect the results (see for example Ramms et al. (7), who study cell mechanics depending on cell IF content). In addition, our analysis aims at comparing two cell types that are handled in the same experimental conditions: temperature, among other parameters, should be the same, but its value is not so important. Sensitivity was determined using a force curve on the supposed infinitely rigid polystyrene. A typical value was 100 nm/V.

We selected cells that were rather elongated (Fig. 1 A), indicating that they were not about to divide, and were distant from each other, so they did not interact and did not result from the same recent cellular division. Measured points were in the cytoplasm around the nucleus (so that cell width was at its highest value), but not above it. For each cell, we took measurements at four different locations.

Reproducibility of measurements of elastic moduli was tested for different cells. In total, hundreds of points were measured per cell type. Maximum indentation depth was ~1 μm, which was less than one-fifth of the overall cell height, a condition that is required for the effect of the rigid substrate to be negligible on total elastic modulus (31). Note that the average maximum cell height was ~6 μm as roughly evaluated from confocal microscopy based on actin location. For each experiment with the three types of cells, the same probe was used whenever possible.

Using the Hertz model, it was possible to infer elastic modulus from the force curve obtained at each point on the cell: this curve represents deflection ( $d$ ) of the cantilever as a function of its vertical displacement ( $z$ ) (Fig. 1 B). From  $d$ , loading force between the cantilever and sample was calculated as  $F = k_C d$ , where  $k_C$  is the cantilever spring constant. For the Hertz model to be valid for the contact tip-sample, the following assumptions were required: materials in contact should be homogeneous and isotropic; contact should be without friction or adhesion; tip should be much stiffer than the sample; and deformations should be small. In practice, the Hertz model was applied although not all assumptions were necessarily met. In the case of contact between a sphere and a flat sample, force is (16):

$$F = k_C d = \frac{4E}{3(1-\nu^2)} \sqrt{R} \delta^{3/2}$$

where  $E$  is Young's modulus,  $\nu$  is Poisson ratio ( $\nu = 0.5$  is usually used for cells, indicating they are incompressible (32)),  $R$  is radius of the sphere, and  $\delta$  is indentation depth and follows  $\delta = z - d$ . Young's modulus ( $E$ ) could then be determined from slope of the plot of  $d^{2/3}$  as a function of  $\delta$  (Fig. 1 C).

In this process, an important issue was determination of the contact point ( $\delta = z - d = 0$ ) because experimentally, there is always an offset both in  $d$  and  $z$ . Indeed, the probe goes through the medium whilst approaching the cell. During this approach, deflection should be zero, but is often observed to be proportional to  $z$ . We presumed that contact occurred when the slope showed a sudden increase (33). This increase can be observed on each force curve, but it would have been very tedious to determine contact points by hand. Therefore, we wrote a program for that purpose (Fig. S2) and performed it using the formal language calculator Mathematica (Wolfram Research, Champaign, IL). Determination of contact points was very subtle. The main difficulty lies in the fact that the probe often oscillates before contact, so the program must detect and analyze these oscillations through successive methods. First, in the region before contact, the effective deflection curve was compared to the linearized one obtained by regression analysis using the least squares method, which also determined both the slope and extension of the region before contact. Second, this extension was optimized (by try and go and other refined methods). Mean oscillation amplitude was also calculated, and it decreased during the approach, so its final value gave an uncertainty estimation to apply for the change of slope detection.

We also added a constant error that represented the noise level. Although this supplementary error could be drastically reduced in many cases, its value was kept constant, allowing the program to automatically treat a large amount of data simultaneously (~100 curves in a few minutes). We also introduced cautiousness strategies: initial and final points were excluded for all linearization processes, and the number of excluded points was fixed to maximize number of curves and quality of contact point determination. Quality of determinations was excellent for more than 95% of data and the calculated contact point was at exactly the same position as seen on the curve.

## AFM mechanical mapping

Mechanical mapping was performed with a Nanowizard 3 AFM (JPK Instruments AG, Berlin, Germany) coupled to an inverted optical microscope with 10× magnification (Nikon, Tokyo, Japan), which allowed positioning of the cantilever on the cell. All measurements were performed with a PFQNM-LC cantilever (Bruker, Billerica, MA) with a nominal spring constant of 0.03 N/m and a conical tip half-angle of 15°. Photodiode sensitivity and

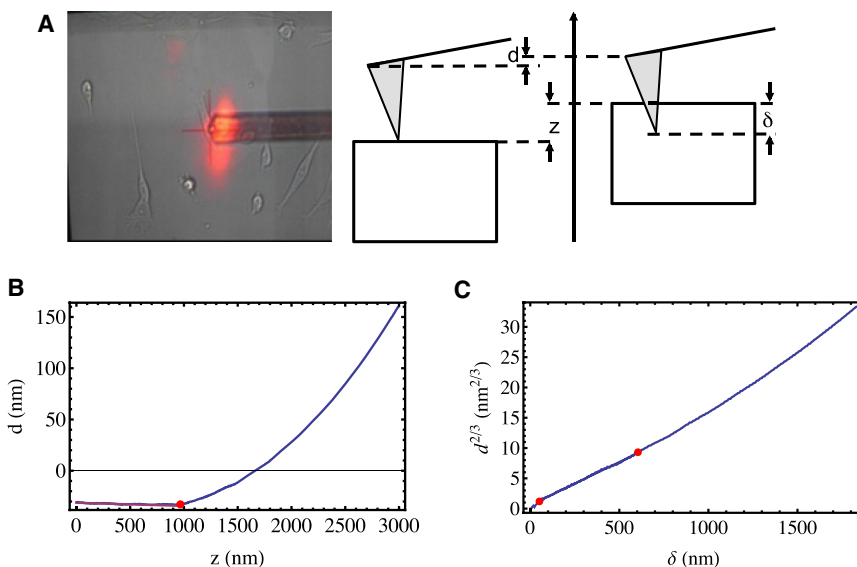


FIGURE 1 Elasticity measurements of cells using AFM. (A) (left) Optical micrographs of myoblasts and the spherical-tipped AFM cantilever, showing the laser that allows deflection measurement. (right) Schematic depicting deflection of the cantilever,  $d$ ; piezo displacement,  $z$ ; and indentation depth,  $\delta$ . (B) Example of an experimental curve providing the deflection,  $d$  (in nm), as a function of displacement,  $z$  (in nm). Linear fit for the first horizontal part of the curve and determined contact point appear in red. (C) Experimental example of  $d^{2/3}$  as a function of the indentation depth,  $\delta$ . Red points indicate the range in which elastic modulus was calculated.

cantilever spring constant were calibrated before every experiment. All measurements were carried out in pre-warmed CO<sub>2</sub>-independent medium. Each sample was kept under the AFM for a maximum of 2 h and the medium was regularly replaced to avoid evaporation. Mechanical maps were obtained by performing 128 × 128 force curves over a scan area of 1600 μm<sup>2</sup>. The z-movement was set to 4 μm with a speed of 100 μm s<sup>-1</sup> and a force set-point of 4 nN. Data processing and analysis were performed with a custom algorithm written in MATLAB (The MathWorks, Natick, MA). We calculated Young's modulus using a model for conical indenters, which calculates force (34):

$$F = \frac{E}{1 - \nu^2} \frac{2 \tan \alpha}{\pi} \delta^2$$

where  $E$  is Young's modulus,  $\alpha$  is half-angle of the cone,  $\delta$  is indentation depth, and  $\nu$  is Poisson's ratio, which was assumed to be 0.5 for incompressible materials.

To investigate variation of elastic properties due to desmin mutation and aggregation, we only considered the perinuclear area. Because this area is several microns in height, no bottom effect correction was necessary (35).

## Western blotting analysis

Proteins were extracted using radioimmunoprecipitation assay buffer without sodium dodecylsulfate, separated by sodium dodecyl sulfate polyacrylamide gel electrophoresis, and transferred to nitrocellulose membranes (GE Healthcare), which were first incubated with 5% milk proteins in 0.5% Tween/phosphate-buffered saline. Primary antibodies were then diluted in solution and incubated for 1 h at room temperature to 16 h at 4°C. Primary antibodies used were 1:500 rabbit polyclonal anti-desmin (Sigma-Aldrich), 1:2000 mouse monoclonal anti- $\alpha$ -actin (Millipore, Billerica, MA), and 1:1000 rabbit polyclonal anti-glyceraldehyde-3-phosphate dehydrogenase (GAPDH) (Sigma-Aldrich). Membranes were then incubated with 1:10,000 isotype-specific secondary antibody coupled to horseradish peroxidase (Pierce; Thermo Fisher Scientific, Waltham, MA). Proteins were visualized by incubating membranes with electrochemiluminescence+ chemiluminescence substrate (GE Healthcare) and photographed with a FUJI Las 4000 charge coupled device camera (GE Healthcare). Quantification of total desmin expression or exogenous versus endogenous desmin ratio were calculated with ImageJ software (National Institute of Health, <https://imagej.nih.gov/ij>). Actin and GAPDH were used as loading controls. Actin was also used for normalization.

## Statistics

Statistics were performed with R free software (R foundation, <https://www.r-project.org/foundation>), which was also used for boxplot representations. Because most values did not exhibit normal (Gaussian) distributions, adapted nonparametric tests were used. Tests were performed using a statistical significance level of 5%. At least three independent experiments were performed. Depending on the experiment,  $n$  represents the number of cells (at least 100 cells were counted for area analysis and stiffness analysis) or number of experiments (western blot analysis).

## RESULTS

### Effect of p.D399Y desmin mutation on cell stiffness

To study the influence of p.D399Y on myoblast stiffness, we performed AFM indentation measurements on a total of 106 DesWT cells, 149 DesMUT cells, and 67 control C2C12 cells, obtained over seven different experiments on freshly prepared live cells under passage 8. Young's moduli distri-

butions for DesWT, DesMUT, and control C2C12 cells were broad: values of elastic moduli varied roughly between 0.5 and 4 kPa (Fig. 2 A). Distributions were clearly non-Gaussian, since they were skewed, and actually followed a log-normal distribution. This behavior is often found for biological processes (36).

Fitting the data to a log-normal distribution allowed us to extract quantitative parameters. Logarithm of the elastic modulus ( $E$ ) followed a normal distribution, from which mean, median and SD could be calculated. Median is more relevant than mean for an asymmetric distribution. Table 1 summarizes the parameters characterizing distributions of the three sets of cells. The difference between medians of C2C12 and DesWT cells was small although western blot analysis showed 2.5-fold desmin overexpression compared to controls (Fig. 2 B and C).

The small difference in Young's moduli for control C2C12 cells and DesWT cells was not statistically significant, as shown by a nonparametric statistical test applied to the two distributions. On the other hand, Young's moduli significantly differed between DesWT and DesMUT cells (Table 1), although desmin expression levels did not significantly differ (Fig. 2 B and C). The median difference in Young's moduli was 39% higher for DesMUT cells than DesWT cells. Skewness, which characterizes asymmetry of the distribution, was highest for DesMUT cells, indicating that DesMUT moduli had the largest amount of high values.

Medians and SDs of Young's moduli showed that DesMUT cells were stiffer than DesWT cells (Fig. 3 A). To further our analysis, we averaged experimental curves and plotted mean force as a function of indentation depth ( $\delta$ ) for DesWT and DesMUT cells (Fig. 3 B). Force ( $k_c d$ ) from the previous Hertz formula was plotted against indentation depth ( $\delta = z-d$ ) for each point in the linear zone where the Hertz model was valid, but also for all points in the approach phase of the probe. As IFs were mainly located relatively deep inside the cell (Fig. S3), the difference between DesWT and DesMUT cells was more prominent at high penetration depths (Fig. 3 B). This difference increased with penetration depth, especially for values greater than  $\sim 1 \mu\text{m}$ .

The two force curves significantly diverged when indentation depth increased to  $\sim 1.8 \mu\text{m}$ . At a depth of  $\sim 0.4 \mu\text{m}$ , nearly 1.6 times higher force was required to indent DesMUT cells than DesWT cells. At  $1.8 \mu\text{m}$ , this ratio was 1.8. As other components of the cytoskeleton were similar in the two cell types, it is reasonable to attribute this effect to the desmin network.

### Effect of desmin aggregates on cell elasticity

p.D399Y mutation forms protein aggregates that can be found in diseased muscle (24). To evaluate the direct contribution of these aggregates to cell elasticity, we used a heat-shock procedure that leads to a high amount of aggregation in p.D399Y mutant cells (27). We performed

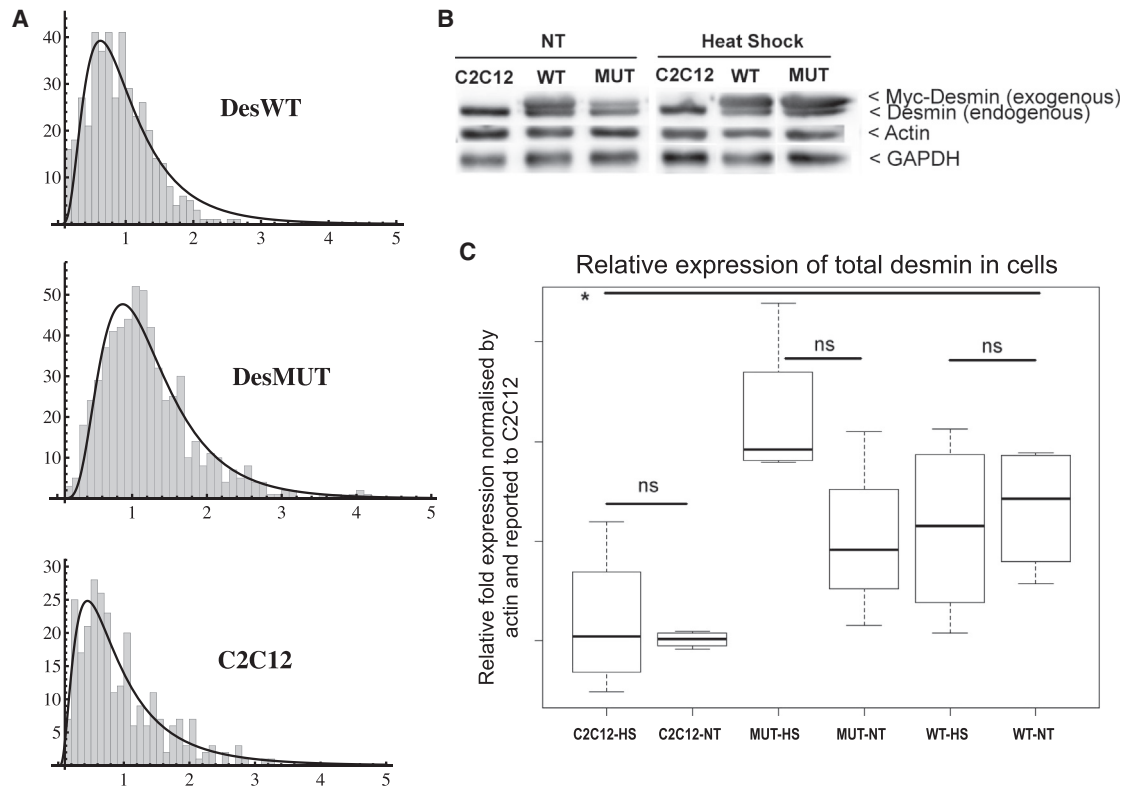


**FIGURE 2** Mutant desmin overexpression increases cell stiffness. (A) Log-normal distributions of Young's moduli for DesWT cells, DesMUT cells, and control C2C12 cells, indicating cell stiffness. (B) Western blot analysis of endogenous or Myc-tagged human desmin expression in inducible stable cell lines 72 h after induction and 24 h after cells were nontreated (NT) or heat-shocked (HS).  $\alpha$ -actin and GAPDH are loading controls. (C) Quantification of total desmin using ImageJ software. Actin was used to normalize protein levels. C2C12 control value was set to 1.0. Results represent three independent experiments. ns, not significant. To see this figure in color, go online.

AFM experiments on heat-shocked C2C12, DesWT, and DesMUT cells and found that heat-shocked DesMUT cells displayed increased aggregation (Fig. 4).

Because mechanical properties are linked to the actin network, we also investigated  $\alpha$ -actin organization. Actin networks and cell areas were not noticeably impacted by desmin expression (Fig. S4 A and B). Similarly, as previously reported (27), desmin overexpression did not affect the presence of steady-state fiber stress. Moreover, the presence of large aggregates in heat-shocked cells did not disrupt the actin network, and no colocalization was detectable (Fig. S4 B).

In AFM experiments on heat-shocked cells, we analyzed 187 DesWT cells, 250 DesMUT cells, and 119 C2C12 cells in eight different experiments. Once more, we obtained

**TABLE 1** Parameters from Log-Normal Distributions of Young's Moduli for DesWT, DesMUT, and C2C12 cells

	DesWT	DesMUT	C2C12
Number of points	425	597	268
Mean (kPa)	0.92	1.23	0.95
Median (kPa)	0.77	1.07	0.74
SD (kPa)	0.61	0.70	0.75
Skewness	0.68	1.38	1.19

log-normal distributions of Young's moduli (Fig. 5, A and B). In these conditions, C2C12 and DesWT cells did not significantly differ (Table 2). Heat-shock treatment increased stiffness of DesWT cells by 60% and increased stiffness of DesMUT cells by 20%. Surprisingly, differences between DesWT and DesMUT cell median moduli were reduced compared to nontreated cells, with DesMUT cell median only slightly higher (10%) than DesWT cell median. Statistical nonparametric tests applied to the three distributions of Young's moduli showed that, after heat stress, DesMUT were still stiffer than DesWT cells. Further, an additional secondary peak appeared for higher Young's moduli in DesMUT cells (Fig. 5 C); this extra peak had no consequence on the main peak position (Fig. 5, A and C). This peak likely arose from desmin aggregates, because it was absent in DesWT and C2C12 cells. To confirm this assumption, stiffness maps were acquired with AFM at higher resolution, and the same cells were fixed at the end of the indentation, stained, and imaged to locate possible aggregates. Desmin aggregates were clearly visible, and corresponding stiffness maps showed stiffer zones at the aggregate areas (Fig. 6). We thus concluded that aggregates were stiffer zones of the cell and were responsible for the secondary peak observed in

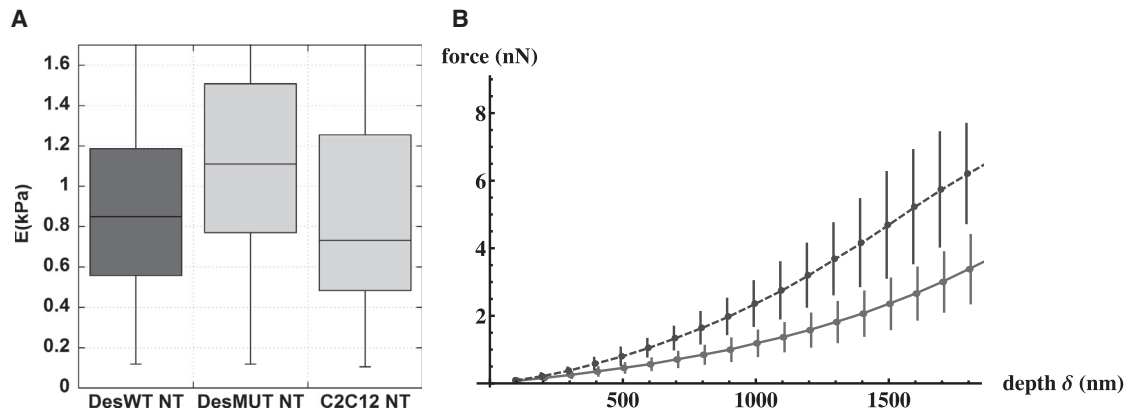


FIGURE 3 Nontreated DesMUT cells are more rigid. (A) Boxplot of Young's moduli of nontreated (NT) DesWT, DesMUT, and C2C12 cells. Boxes are twice the size of the standard deviation. (B) Force as a function of indentation depth,  $\delta$ , averaged on experimental curves. Dotted curve corresponds to DesMUT cells (29 curves), whereas solid line corresponds to DesWT cells (37 curves). Error bars represent median deviations. To see this figure in color, go online.

the DesMUT distribution. For heat-shocked cells, a plot of force as a function of depth showed that there was no separation between force for heat-shocked DesWT and DesMUT cells (Fig. S5).

## DISCUSSION

In this study, we show that myoblasts expressing p.D399Y mutant desmin are significantly stiffer than WT myoblasts. In contrast, overexpression of WT desmin does not significantly affect Young's modulus in comparison to control C2C12 cells. These results are in agreement with our previous data from cyclic cell stretching (4) where we showed that dynamics of cell reorientation and morphology adjustments to overcome mechanical stress are less efficient in

DesMUT cells. Cell stiffness may reduce or slow down the adaptation of cells to mechanical stretch. Indeed, when adherent cells are cyclically stretched through deformable substrates, they change their orientation (4). For high frequencies, cells align in a direction nearly perpendicular to the stretching direction. p.D399Y mutation in desmin alters this behavior, leading to slower dynamics of reorientation and reduction of the orientation angle. We hypothesize that stiffer cells are less deformable under stretching. Therefore, they are less likely to accomplish the needed rearrangements with the same velocity as normal cells. In fact, the reorientation process takes place by gradually changing cell morphology. Stiffer cell morphology changes probably require more energy, in agreement with our previous results showing that DesMUT cell morphology changes take longer than those of DesWT cells (4).

How do changes in mechanical or dynamical properties at the cell scale result from molecular scale alterations, such as IF mutations? We speculate that the effect may be related to desmin filament stiffness inside the cell or to the impact of alterations in mechanotransduction. The first hypothesis is supported by Kreplak and Bär (28), who studied the effects of many desmin mutations on the elasticity of single desmin filaments in vitro. In particular, p.D399Y mutation increases elasticity at a single-filament level, whereas A360P mutation preserves a softness similar to nonmutated filaments. Filament properties are defined by their quaternary structure, and a mutation in the rod part of the sequence, like p.D399Y, can likely affect this structure. Hence, when the desmin network is built from rigid molecular structures, its elasticity as a whole can change. This could explain increased elasticity at a whole-cell level in mutant cells.

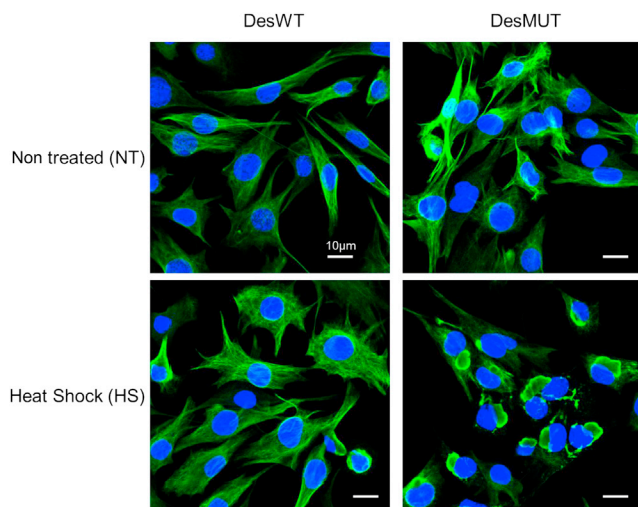


FIGURE 4 Heat-shock treatment increases desmin aggregation in DesMUT cells. Representative micrographs of immunostained nontreated (NT) and heat-shocked (HS) DesWT and DesMUT cells 24 h after treatment. Cells were stained for Myc-tagged desmin (green) and Hoechst nuclear dye (blue). White scale bar indicates 10  $\mu$ m. Crop without zoom of a  $5 \times 5$  tile scan taken with a  $40\times$  objective (numerical aperture = 0.95).

## Rough value of Young's modulus

In this study, the order of magnitude of Young's modulus is, for all cells and in all cases, 1 kPa. However, Young's modulus for C2C12 cells has been reported to be 11 kPa

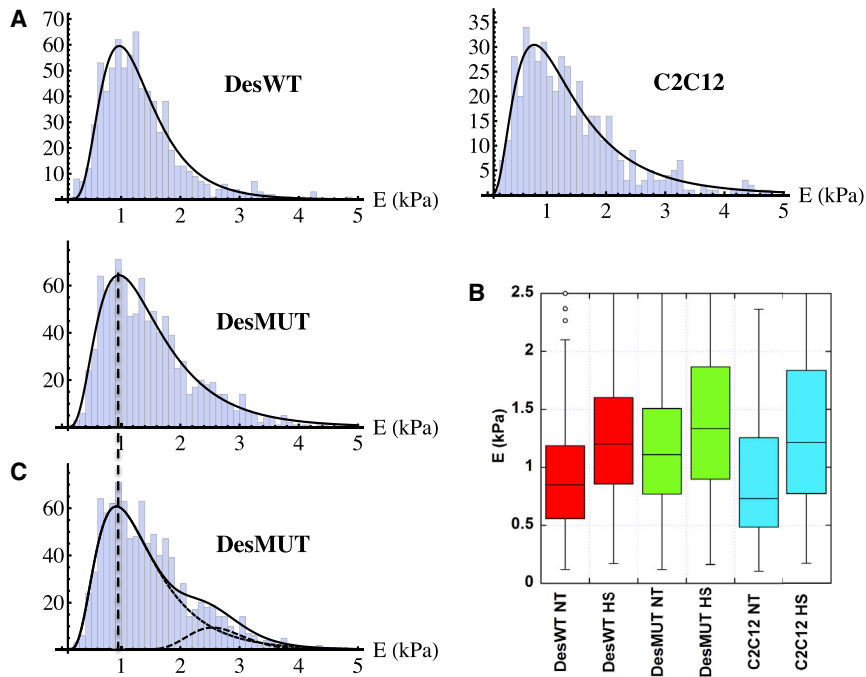


FIGURE 5 Young's moduli for heat-shocked cells. (A) Obtained log-normal distributions of Young's moduli for heat-shocked DesWT cells, DesMUT cells, and C2C12 cells. (B) Corresponding boxplots of stiffness of nontreated (NT) or heat-shocked (HS) DesWT cells, DesMUT cells, and C2C12 cells. (C) Distribution of Young's moduli of heat-shocked DesMUT cells shows a secondary peak at higher modulus values. To see this figure in color, go online.

(37). The difference might come from using spherical probes instead of pyramidal ones. Indeed, it is well known that Young's modulus values on the same cells are higher for pyramidal tips than for spherical probes (38). In comparison, untransfected control fibroblasts have a Young's modulus of 2.55 kPa (10), which is in the same order of magnitude as our results with C2C12 cells (1.05 kPa). Once again, the difference might come from the use of pyramidal probes (10) instead of spherical ones. Another possibility is that this difference could arise from cell differences between myoblasts and fibroblasts. Hence, one has to pay attention to tip geometry and cell type when comparing data from different experiments.

### Effect of p.D399Y desmin mutation

Our results show that desmin-mutated cells are 39% more rigid than WT cells. Elastic moduli were measured using only the first part of the force curves, i.e., for low depth values (up to 0.4  $\mu\text{m}$ ). However, curves of force as a function of depth revealed that DesMUT cells appear more rigid than DesWT cells for depth values of 0.5–1.8  $\mu\text{m}$ . IFs are more concentrated deep in the cell, so it is natural for elasticity differences to appear more pronounced at such values of depth. This confirms previous results that show that, in the cell body, the difference between keratin-deficient and WT keratinocytes increases as depth increases and becomes significant starting at a certain value (7). Our results are also in agreement with Guo et al. in embryonic fibroblasts (39). Comparing WT to vimentin-deficient fibroblasts, they showed that vimentin IFs stiffen the cytoplasm by doubling its shear modulus but do not significantly affect the cell cor-

tex. Here, the difference is more subtle, but we used WT and desmin-mutated cells rather than WT and desmin-deficient cells, which would have resulted in more drastic differences. Our cells also expressed endogenous WT IFs, which could have reduced the effect of the mutation on elasticity change.

Actin plays a major role in the elasticity of cells (11,17). Our results, by measuring a difference in elasticity between DesWT and DesMUT cells, show that IFs also play a role in cell elasticity. This confirms the results of previous studies (10,39–42), although our data provide more direct information. For instance, cells expressing some mutated desmin present increased stiffness (10), but these results come from fibroblasts transfected with WT or mutated desmin, which is not physiologically expressed in fibroblasts. In contrast, we used inducible cell lines derived from an isogenic C2C12 myoblast background expressing WT or mutated desmin. The first advantage of our stable expression is to minimize the effect of overexpression. Indeed in transient expression, transfection concerns only a few cells (30% in C2C12), presenting a high rate of expression that can lead to artifactual aggregation even for WT desmin

TABLE 2 Parameters from Log-Normal Distributions of Young's Moduli for Heat-Shocked DesWT, DesMUT, and C2C12 cells

	DesWT	DesMUT	C2C12
Number of points	748	1001	478
Mean (kPa)	1.33	1.90	1.44
Median (kPa)	1.18	1.30	1.18
SD (kPa)	0.70	0.84	1.01
Skewness	1.64	1.13	2.37

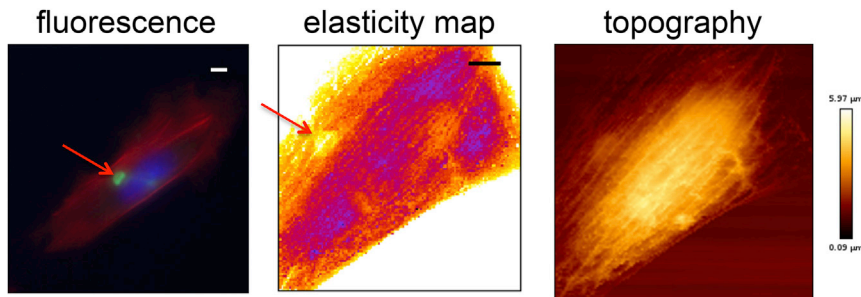


**FIGURE 6** Desmin aggregates in heat-shocked DesMUT cells correspond with increased cell stiffness. Corresponding fluorescence, elasticity map, and topographic images of the same heat-shock-treated DesMUT cell. Fluorescence image (left) shows staining with F-actin (red), Myc-tagged desmin (green), and 4',6-diamidino-2-phenylindole nuclear staining (blue). Image taken with a 10 $\times$  objective. Elasticity map (center) shows Young's moduli with lowest values in blue, intermediate values in red, and high values in yellow. The Scale bar represents 5  $\mu$ m. Topography image (right). Arrows indicate the aggregate that is present in the cell.

(27). Moreover, the rate of expression in transient experiments is  $\sim$ 9:1 for exogenous human desmin compared to endogenous murine desmin (Fig. S6). However, our stable clones expressed a ratio of  $\sim$ 1:1 (27) and all cells expressed the exogenous protein at similar levels. Establishing stable clones also allowed us to avoid the deleterious cell membrane effects of lipofection agents, which are known to affect cells' mechanical properties and responses.

### Effect of WT desmin expression

C2C12 cells express a small amount of endogenous desmin, whereas DesWT cells stably express 2-fold WT murine endogenous + human exogenous desmin. Interestingly, we measured only a slight, although nonsignificant, increase in cell stiffness between control C2C12 and DesWT cells. However, previous studies have found conflicting results.

Plodinec et al. (10) found that desmin-transfected fibroblasts are 35% softer than untransfected fibroblasts. However, the authors compared mean values of Young's moduli, whereas we used medians of the distributions, which is required for non-Gaussian processes. Moreover, Plodinec et al. used a Student's *t*-test to perform statistical analysis, whereas we used a nonparametric test. In principle, the Student's *t*-test should be used only when distributions are Gaussian, which is clearly not the case. Moreover, it is not straightforward to compare desmin's effects on fibroblasts to those of myoblasts, because desmin is not a naturally expressed IF in fibroblasts and because the mechanical properties of fibroblasts may differ from myoblasts due to their different biological functions.

In contrast, using optical tweezers, Charrier et al. (6) found that C2C12 cells transiently transfected with WT desmin are 33% stiffer than nontransfected cells. However, it is important to emphasize that these studies used electroporation to transiently express desmin. Transfection is known to rigidify cell membranes, and thus may introduce a bias in comparison with nontransfected cells, as we did. Charrier et al. found that desmin overexpression was around 2:1 of exogenous vs endogenous desmin, which is higher than the 1:1 expression that we measured

in the stable clones. Therefore, even if the increased stiffness we measured is partly due to desmin overexpression, we can assume that the lower desmin content in our case was insufficient to induce a significant change in stiffness.

### Effect of desmin aggregates

A small percentage (around 5% maximum) of DesMUT cells contain aggregates of desmin (27). More generally, desminopathy is characterized by the presence of desmin aggregates in muscle fibers. Thus, the enhanced stiffness of DesMUT cells compared to DesWT cells could be due to aggregates. To measure the contribution of these aggregates to cell stiffness, we heat-shocked cells to increase desmin aggregation. Heat-shock is reported to induce up to 93% aggregates in DesMUT cells after 24 h (27). On average, our experiments measured up to 60% aggregation, although these differences could be due to sensitivity to experimental variations.

If aggregates significantly affect cell stiffness, the difference between DesWT and DesMUT cells should be greatly enhanced when cells are heat-shocked. However, we did not observe as robust a difference after heat-shock treatment as might be expected given the difference in aggregate percentage. Indeed, the difference between heat-shocked DesWT and DesMUT was statistically relevant, but median Young's modulus of DesMUT cells was only 10% higher than that of DesWT cells. In addition, stiffness of all cells increased by 20–60% due to heat-shock treatment. Therefore, heat-shock itself has an effect on cell stiffness that is greater than that of aggregates.

The effect of desmin aggregates is nonetheless evident because we observed a secondary peak at high values of Young's moduli only for DesMUT cells. Further, stiffness maps showed that aggregates were stiffer than the rest of the cell. We can thus conclude that the observed secondary peak is due to aggregates. We may then hypothesize that, in the case of nontreated cells, aggregates that are too small to be detected with fluorescence microscopy may be present and may contribute to the higher elasticity values measured for nontreated mutated cells.

## CONCLUSIONS

In this work, we show that p.D399Y-mutant desmin expression in myoblasts significantly increases the cells' elastic moduli. This is true for elastic moduli measured at low values of depth, where the Hertz model applies. Moreover, differences in stiffness between cells expressing WT or mutated desmin are more pronounced with increasing cell depth. This suggests that deep inside the cell, where deformation is higher, the contribution of IFs is higher. On the other hand, we also show that aggregates are stiffer zones of the cell, supporting the assumption that aggregation contributes to increased cell rigidity. Additionally, increased stiffness of all cells as a consequence of heat-shock stress is an interesting and, to our knowledge, new result that needs further investigation in the future.

## SUPPORTING MATERIAL

Six figures are available at [http://www.biophysj.org/biophysj/supplemental/S0006-3495\(17\)30670-7](http://www.biophysj.org/biophysj/supplemental/S0006-3495(17)30670-7).

## AUTHOR CONTRIBUTIONS

F.B., S.B.-P., C.E., F.D., and P.V. conceived the experiments. C.E., F.D., A.F.R., V.B., and A.d.S.M. performed the experiments. C.E., G.A., F.B., F.D., A.F.R., and F.R. analyzed the data. F.B., C.E., and S.B.-P wrote the manuscript.

## ACKNOWLEDGMENTS

We are grateful to E. Raspaud for careful review of the manuscript and useful comments. We thank J. Doucet for fruitful discussions. We acknowledge funding from the Agence Nationale de la Recherche (13BSV5-0017-DESMECA) and from the Association Française contre les Myopathies: AFM 15454. Confocal pictures were performed at the Plateau d'imagerie of the BFA unit.

## REFERENCES

1. Wu, H. W., T. Kuhn, and V. T. Moy. 1998. Mechanical properties of L929 cells measured by atomic force microscopy: effects of anticytoskeletal drugs and membrane crosslinking. *Scanning*. 20:389–397.
2. Fletcher, D. A., and R. D. Mullins. 2010. Cell mechanics and the cytoskeleton. *Nature*. 463:485–492.
3. Grady, M. E., R. J. Composto, and D. M. Eckmann. 2016. Cell elasticity with altered cytoskeletal architectures across multiple cell types. *J. Mech. Behav. Biomed. Mater.* 61:197–207.
4. Leccia, E., S. Batonnet-Pichon, ..., F. Briki. 2013. Cyclic stretch reveals a mechanical role for intermediate filaments in a desminopathic cell model. *Phys. Biol.* 10:016001.
5. Russell, D., P. D. Andrews, ..., E. B. Lane. 2004. Mechanical stress induces profound remodelling of keratin filaments and cell junctions in epidermolysis bullosa simplex keratinocytes. *J. Cell Sci.* 117:5233–5243.
6. Charrier, E. E., A. Asnacios, ..., S. Hénon. 2016. Desmin mutation in the C-Terminal domain impairs traction force generation in myoblasts. *Biophys. J.* 110:470–480.
7. Ramms, L., G. Fabris, ..., B. Hoffmann. 2013. Keratins as the main component for the mechanical integrity of keratinocytes. *Proc. Natl. Acad. Sci. USA*. 110:18513–18518.
8. Strelkov, S. V., H. Herrmann, and U. Aebi. 2003. Molecular architecture of intermediate filaments. *BioEssays*. 25:243–251.
9. Qin, Z., L. Kreplak, and M. J. Buehler. 2009. Hierarchical structure controls nanomechanical properties of vimentin intermediate filaments. *PLoS One*. 4:e7294.
10. Plodinec, M., M. Loparic, ..., C. A. Schoenenberger. 2011. The nanomechanical properties of rat fibroblasts are modulated by interfering with the vimentin intermediate filament system. *J. Struct. Biol.* 174:476–484.
11. Petersen, N. O., W. B. McConnaughey, and E. L. Elson. 1982. Dependence of locally measured cellular deformability on position on the cell, temperature, and cytochalasin B. *Proc. Natl. Acad. Sci. USA*. 79:5327–5331.
12. Duszyk, M., B. Schwab, 3rd, ..., E. L. Elson. 1989. Cell poking: quantitative analysis of indentation of thick viscoelastic layers. *Biophys. J.* 55:683–690.
13. Evans, E. A. 1989. Structure and deformation properties of red blood cells: concepts and quantitative methods. *Methods Enzymol.* 173:3–35.
14. Discher, D. E., N. Mohandas, and E. A. Evans. 1994. Molecular maps of red cell deformation: hidden elasticity and in situ connectivity. *Science*. 266:1032–1035.
15. Hildebrand, J. A., and D. Rugar. 1984. Measurement of cellular elastic properties by acoustic microscopy. *J. Microsc.* 134:245–260.
16. Radmacher, M. 2002. Atomic Force Microscopy. In *Cell Biology*. J. K. H. Hörber and B. P. Jena, eds. (Academic Press), pp. 67–90.
17. Kuznetsova, T. G., M. N. Starodubtseva, ..., R. I. Zhdanov. 2007. Atomic force microscopy probing of cell elasticity. *Micron*. 38: 824–833.
18. Ikai, A. 2010. A review on: atomic force microscopy applied to nanomechanics of the cell. *Adv. Biochem. Eng. Biotechnol.* 119:47–61.
19. Lekka, M., D. Gil, ..., P. Laidler. 2012. Cancer cell detection in tissue sections using AFM. *Arch. Biochem. Biophys.* 518:151–156.
20. Cross, S. E., Y. S. Jin, ..., J. K. Gimzewski. 2007. Nanomechanical analysis of cells from cancer patients. *Nat. Nanotechnol.* 2:780–783.
21. Coughlin, M. F., D. R. Bielenberg, ..., J. J. Fredberg. 2013. Cytoskeletal stiffness, friction, and fluidity of cancer cell lines with different metastatic potential. *Clin. Exp. Metastasis*. 30:237–250.
22. Bastatas, L., D. Martínez-Marín, ..., S. Park. 2012. AFM nano-mechanics and calcium dynamics of prostate cancer cells with distinct metastatic potential. *Biochim. Biophys. Acta*. 1820:1111–1120.
23. Schopferer, M., H. Bär, ..., N. Willenbacher. 2009. Desmin and vimentin intermediate filament networks: their viscoelastic properties investigated by mechanical rheometry. *J. Mol. Biol.* 388:133–143.
24. Goldfarb, L. G., P. Vicart, ..., M. C. Dalakas. 2004. Desmin myopathy. *Brain*. 127:723–734.
25. Goudeau, B., F. Rodrigues-Lima, ..., P. Vicart. 2006. Variable pathogenic potentials of mutations located in the desmin alpha-helical domain. *Hum. Mutat.* 27:906–913.
26. Kreplak, L., H. Bär, ..., U. Aebi. 2005. Exploring the mechanical behavior of single intermediate filaments. *J. Mol. Biol.* 354:569–577.
27. Segard, B. D., F. Delort, ..., S. Batonnet-Pichon. 2013. N-acetyl-L-cysteine prevents stress-induced desmin aggregation in cellular models of desminopathy. *PLoS One*. 8:e76361.
28. Kreplak, L., and H. Bär. 2009. Severe myopathy mutations modify the nanomechanics of desmin intermediate filaments. *J. Mol. Biol.* 385:1043–1051.
29. Futai, N., W. Gu, ..., S. Takayama. 2006. Handheld recirculation system and customized media for microfluidic cell culture. *Lab Chip*. 6:149–154.
30. Hutter, J. L., and J. Bechhoefer. 1993. Calibration of atomic-force microscope tips. *Rev. Sci. Instrum.* 64:1868–1873.

31. Domke, J., and M. Radmacher. 1998. Measuring the elastic properties of thin polymer films with the atomic force microscope. *Langmuir*. 14:3320–3325.
32. Mahaffy, R. E., S. Park, ..., C. K. Shih. 2004. Quantitative analysis of the viscoelastic properties of thin regions of fibroblasts using atomic force microscopy. *Biophys. J.* 86:1777–1793.
33. Crick, S. L., and F. C. Yin. 2007. Assessing micromechanical properties of cells with atomic force microscopy: importance of the contact point. *Biomech. Model. Mechanobiol.* 6:199–210.
34. Wang, J. H., and B. P. Thampatty. 2006. An introductory review of cell mechanobiology. *Biomech. Model. Mechanobiol.* 5:1–16.
35. Gavara, N., and R. S. Chadwick. 2012. Determination of the elastic moduli of thin samples and adherent cells using conical atomic force microscope tips. *Nat. Nanotechnol.* 7:733–736.
36. Limpert, E., W. A. Stahel, and M. Abbt. 2001. Log-normal distributions across the sciences: keys and clues. *Bioscience*. 51:341–352.
37. Collinsworth, A. M., S. Zhang, ..., G. A. Truskey. 2002. Apparent elastic modulus and hysteresis of skeletal muscle cells throughout differentiation. *Am. J. Physiol. Cell Physiol.* 283:C1219–C1227.
38. Carl, P., and H. Schillers. 2008. Elasticity measurement of living cells with an atomic force microscope: data acquisition and processing. *Pflugers Arch.* 457:551–559.
39. Guo, M., A. J. Ehrlicher, ..., D. A. Weitz. 2013. The role of vimentin intermediate filaments in cortical and cytoplasmic mechanics. *Biophys. J.* 105:1562–1568.
40. Haga, H., S. Sasaki, ..., T. Sambongi. 2000. Elasticity mapping of living fibroblasts by AFM and immunofluorescence observation of the cytoskeleton. *Ultramicroscopy*. 82:253–258.
41. Bonakdar, N., J. Luczak, ..., B. Fabry. 2012. Biomechanical characterization of a desminopathy in primary human myoblasts. *Biochem. Biophys. Res. Commun.* 419:703–707.
42. Lulevich, V., H. Y. Yang, ..., G. Y. Liu. 2010. Single cell mechanics of keratinocyte cells. *Ultramicroscopy*. 110:1435–1442.